Geological constraints in velocity inversion

Jos van Trier

ABSTRACT

The result of velocity-inversion methods depends on the parametrization of the velocity model and the way it is constrained during the inversion. When a smooth-velocity model is chosen, the velocity inversion can often be performed efficiently, but the risk of finding a non-geological model is severe.

In this paper geological information is used to parametrize the velocity model and to constrain the velocity inversion, leading to a more realistic velocity model. An important part of the geological information comes from interpreting the seismic image of the subsurface. The image is obtained by migration-velocity optimization with a smooth velocity model. The smooth model, resulting from the optimization, correctly models cumulative traveltimes to reflectors.

Structural boundaries are picked from the image, where the boundaries are given a certain width, corresponding to the seismic resolution in the image. The picked boundaries are used to parametrize the velocity model in several structures, each with a velocity function independent of the others. The velocity functions are modeled by splines.

A second optimization determines the velocities inside the structures (the boundaries themselves are kept fixed). The data used in the optimization are the traveltimes of rays traveling from reflectors to the surface through the smooth model. The optimization is damped by geological constraints, coming from well logs and general geological information.

INTRODUCTION

Traditionally, geophysical and geological information have been used separately in seismic exploration: geophysicists process the raw seismic data and produce a seismic image and velocity model of the subsurface; geologists subsequently interpret the image—incorporating the velocity model and extra information (e.g. well

logs)—and identify target zones for oil exploitation. If the velocity model and seismic image were unique, everything would be all right. However, the limited amount of data forces geophysicists to make assumptions in the processing stage. These assumptions often introduce errors into the velocity model, resulting in errors in the seismic image. This can lead to mistakes in the interpretation (dry holes!).

The increase in computing power and the advance of interactive workstations now make it possible to integrate processing and interpretation. Geological information can be used in the processing stage to help the geophysicist in constraining the velocity model. An initial velocity model and its associated seismic image need no longer be considered as end products of seismic processing; the seismic image can be interpreted to further constrain the velocity model. Likewise, well log and other geological information can be used in constraining the velocity model.

More specifically, I propose to apply geological constraints in migration-velocity analysis. Migration-velocity analysis (Fowler, 1985; 1986; Al-Yahya, 1987) is necessary in areas with strong lateral velocity variation and complicated geology. The result of the analysis is a velocity model for which the migrated data are well-focused.

In migration-velocity analysis the velocity model needs to be constrained because of the mentioned non-uniqueness of the solution. Often a smooth model is chosen from the range of possible velocity models. There are several reasons for doing so. Smooth models can be described with only a few parameters, and can therefore be easily determined in an optimization scheme. Also, smooth models generally do not degrade migrations: the positioning of reflectors in migration depends only on integral measures of velocity.

However, smoothness in velocity does limit interpretability of the velocity analysis: for interpretational purposes it is desirable to find a structural velocity model that can be related to geological features. It is possible to specify both velocities and boundaries of the structures as parameters in an optimization, but there are some problems with this approach. First, velocity and depth are different physical parameters that need to be scaled differently in the optimization. The scaling constants are hard to determine in advance, as they are structure-dependent. Second, both the velocity in a layer and the depth of the layer control the position of a reflector after migration. Trying to adjust them both in an optimization method can lead to instabilities and non-convergence of the solution.

If geological constraints are used in the velocity optimization, it is possible to determine structural velocity models while avoiding the above problems. I start with the results of a "smooth model optimization," i.e., a smooth velocity model and a focused seismic image. From the seismic image structure boundaries are picked. The picking is guided by geological knowledge, and, if available, well log information. Now that the structural boundaries are defined, the behavior of the velocity in each structure is determined in a second optimization.

An important question is whether the image of the subsurface generated by migration with a smooth model is accurate enough to pick boundaries. I address this problem by analyzing a synthetic dataset, and propose fuzzy boundaries as a solution. Fuzzy boundaries have a certain width that corresponds to the seismic resolution.

After the smooth-model optimization, traveltimes to reflectors can be correctly modeled with the smooth model (as the goal of this optimization is to find the right position of the reflectors, or, equivalently, the cumulative traveltimes to the reflectors). Now, the structural model is found by a tomographic inversion: rays are traced from the reflectors to the surface, and the traveltimes of the rays are matched with the traveltimes of rays traveling through the smooth model. The structural model is geologically constrained in the inversion by applying a damping matrix, that is constructed from well log and general geological information. The structural model may further be refined and verified by a detailed analysis of the migrated data. I will discuss this analysis in a companion paper (Van Trier, 1988b).

Finally, a remark about the mentioned problems with parametrizing both structure and velocity. Of course, these problems are not unsolvable, especially if the inversion is interactively guided and done by layer stripping. However, when a picking error is made in the early stage of the interactive inversion, the final result may be erroneous. Also, when several iterations are needed to find the right model, this can be time consuming (real time, not necessarily CPU-time). In the method described here, picking is postponed until a well-focused image is available, and human intervention occurs only in one central step, after which all the geological information is combined in the parametrization and constraining factors of the structural-velocity model.

THE METHOD

The method consists of four steps:

1. Determination of smooth velocity model. Several migration-velocity analysis methods have been developed in the last years (Fowler, 1986; Al-Yahya, 1987; Etgen, 1987; Van Trier, 1987). They all give a smooth velocity model as a function of depth. I prefer the methods that use the constant surface location (CSL) gathers after migration, because I want to analyze these gathers later. These methods are based on the fact that events in CSL gathers are flat after migration with the correct velocity, independent of structure.

   Other methods that result in a smooth velocity model (Sword, 1987; Biondi, 1988) may be used as well. However, migration-velocity analysis methods not only produce a smooth velocity model, but also a migrated image and the aforementioned CSL gathers. Analysis of these "side products" is important in the next steps.

2. Geological interpretation. The migrated image is interpreted; structural boundaries are picked, and seismic sequences are identified. At this step geological knowledge is used to define boundaries where velocity contrasts are likely to occur (boundaries of seismic sequences, at intrusions, etc.). The result of this analysis is a structural depth section. If well logs are available, velocities can be further constrained: at the borehole velocities are either known or their fluctuation with depth can be determined. Finally, general geological information, such as regional dip, can be incorporated in the velocity model.

3. Determination of global velocities inside the structural elements. Once the structural boundaries are defined, the velocities inside the structure elements are estimated in a second optimization. The smooth-model optimization of step 1 essentially attempts to match the cumulative traveltimes calculated with the model with the ones found in the seismic data. The same cumulative traveltimes are now used in a tomographic inversion, using a structural velocity model instead of a smooth one, and the model is constrained by the geological observations. To construct a matrix that linearly relates model and traveltimes, rays are traced from the reflectors to the surface. In the optimization the matrix is inverted by a conjugate gradient routine (LSQR).

4. Refining and verifying the structural-velocity model. Residual statics can be done by analyzing CMP gathers after NMO. Similarly, a careful analysis of the depth variation of a reflector in an CSL gather after migration can be used to find local velocity perturbations in the structural model. This part of the optimization is performed almost without extra computational cost: the matrix of step 3 can be used for the inversion.

   Likewise, the ray tracing of step 3 can be used to convert the offset axis in a CSL gather to an angle axis. The behavior of reflection events in the CSL gathers as a function of reflection angle provides the means to verify velocity contrast at those reflectors.

In this paper, I concentrate on the central part of the method: the geological interpretation and determination of global structural velocities. A field-data example of the first part, the smooth-model optimization, and the theory of the last part are subject of two separate articles (Van Trier, 1988b; 1988c).

GEOLOGICAL INTERPRETATION

After the smooth-model optimization the focused depth image is interpreted: structural boundaries are picked, and, if possible, velocities in specific structures are determined. For example, salt structures are normally easy to identify on the migrated image, and the velocity of salt formations in certain sedimentary basins is often known. Other geological information can come from well logs, or general geological knowledge of the area.

An important issue is whether the depth image is accurate enough to pick boundaries. I address this problem in the next section, and I introduce "fuzzy boundaries": boundaries that have a certain width corresponding to the seismic resolution in the migrated image.

Picking of structural boundaries

The smooth-model optimization flattens events in the CSL gathers. Consequently, one can assume that positioning errors in the location of reflectors after migration are small. Still, the accuracy of the seismic image is limited by the width of the seismic wavelet after migration. Also, some parts of the subsurface are well-illuminated by the seismic survey, whereas others are not.

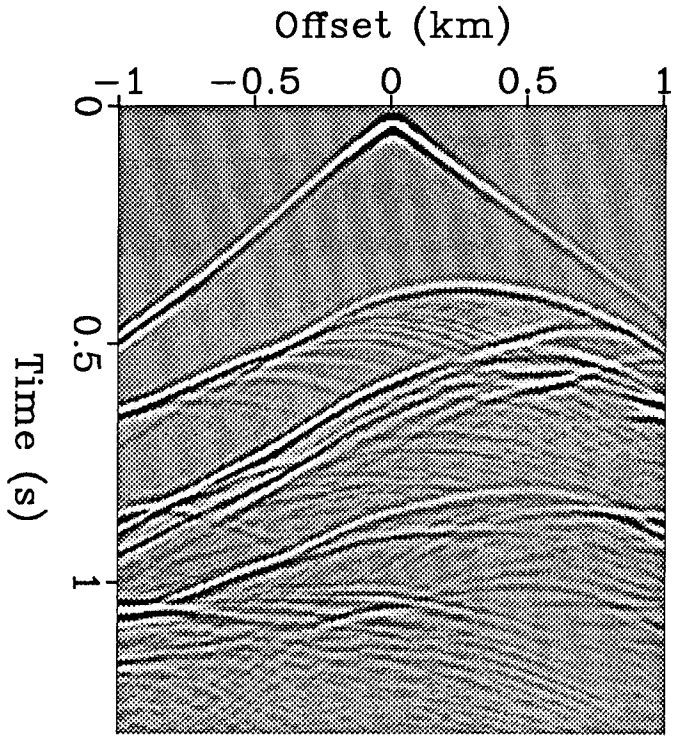

FIG. 1. Shot profile with shot positioned at the surface location of 2 km. The two off-centered hyperbolas in the middle are reflections from the dipping salt intrusion. Diffraction hyperbolas are caused by velocity contrasts in the gridded model.

To test the accuracy of the stacked image after migration with a smooth model, synthetic shot profiles are generated for a structural model and migrated with a smooth model. The migrated profiles are then stacked and the stacked image is compared with the real structure.

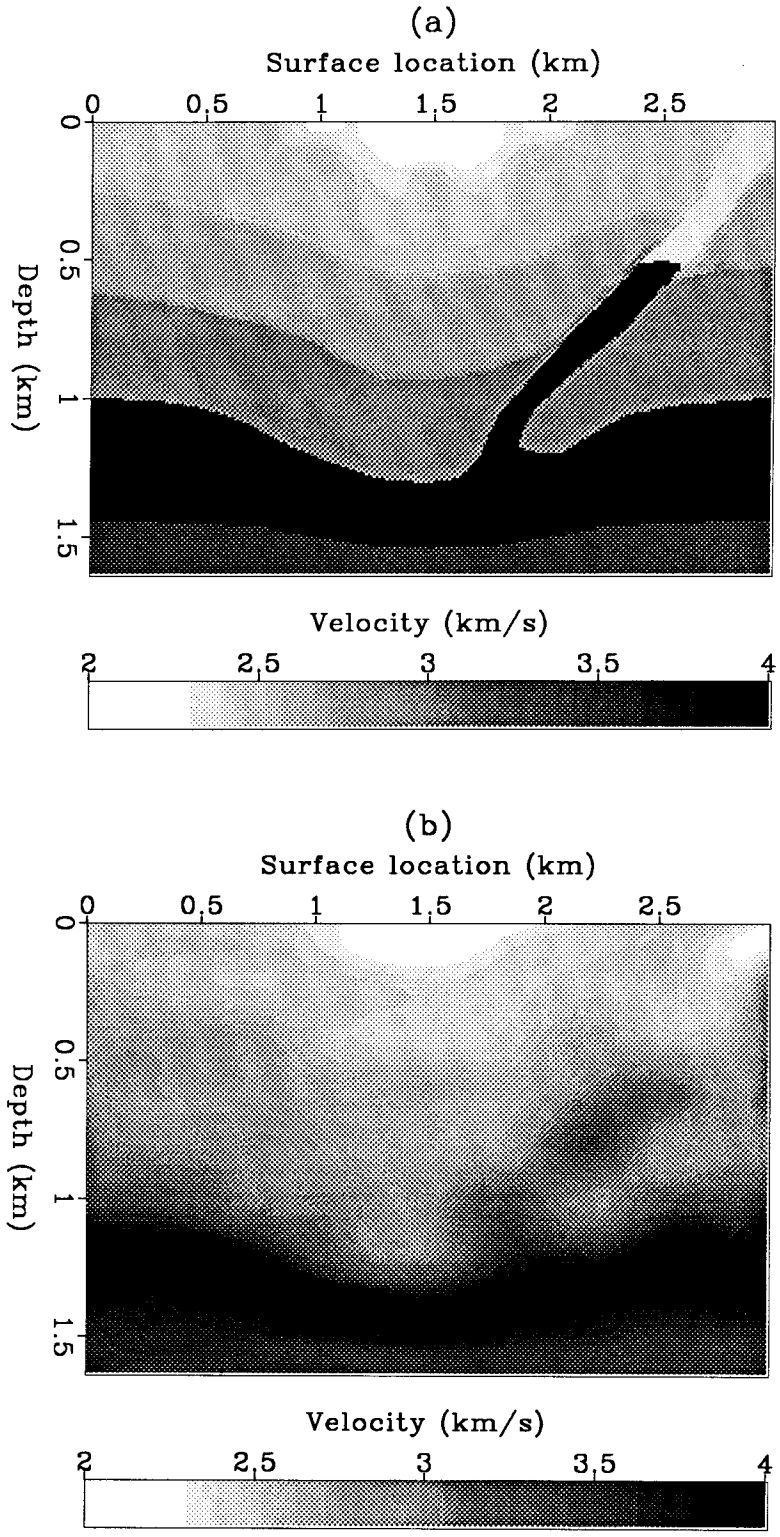

FIG. 2. Structural model (a), and its smooth representation (b).

The synthetic data are calculated with an acoustic finite-difference modeling program. Figure 1 shows an example of a synthetic shot profile. The structural-velocity model used in the modeling is shown in Figure 2a. It contains a syncline with a high-velocity salt intrusion. The structures have constant velocities, except for the top one that has a low-velocity region in the middle. 100 shot profiles are generated, each consisting of 200 traces in a split-spread configuration. The geophone spacing is 10 m, the shot spacing is 20 m. The maximum seismic frequency is 80 Hz. Shot positions range from surface locations 500 to 2500 m.

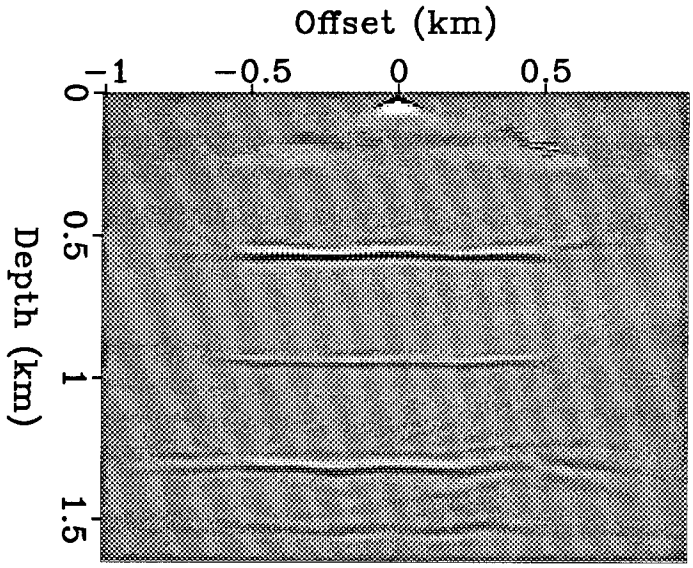

FIG. 3. CSL gather at the surface location of 1.5 km. The 4 events are reflections from the 4 layer boundaries in the syncline.

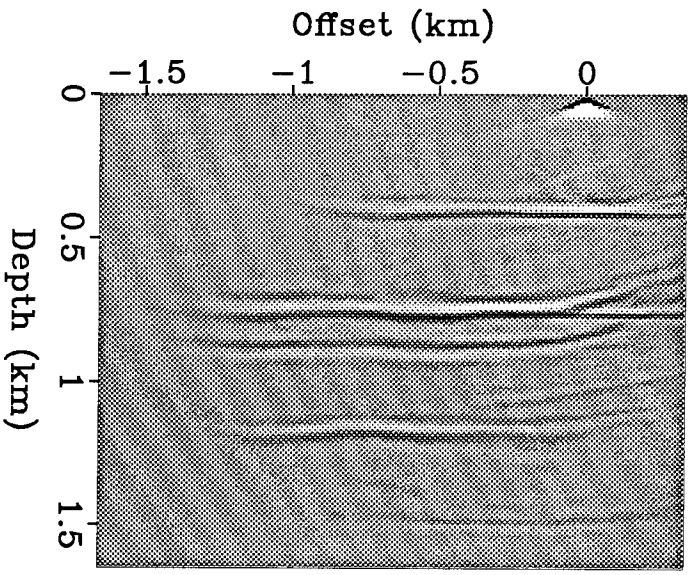

FIG. 4. CSL gather at the surface location of 2.15 km. On top of the 4 events two other events can be seen in the middle part of the gather. The events are reflections from the salt intrusion. They are not centered at zero offset because the intrusion is dipping.

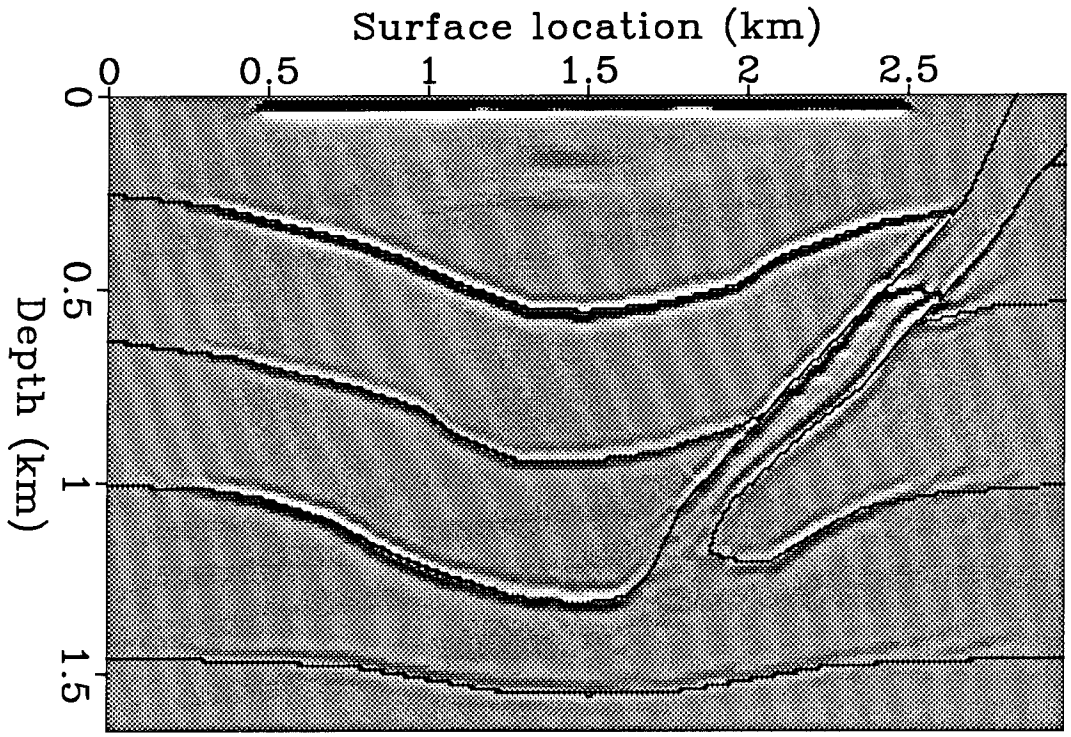

FIG. 5. Seismic image after migration with the smooth model of Figure 2b. The structural boundaries of the true model are plotted on top of the image.

The data are migrated with a Kirchhoff migration program, using the smooth model displayed in Figure 2b. The smooth model is found by fitting two-dimensional spline functions to the true velocity model, where the spline knots are widely spaced (8 knots in both depth and lateral directions). Although the smooth-model optimization is not explicitly done, the shown model is typical and could have been the result of such an optimization: it is represented by only few parameters (the spline coefficients at the knots), and after migration the events in the CSL gathers are more or less flat. For example, Figure 3 shows the CSL gather at the surface location of 1.5 km, Figure 4 displays the CSL gather at 2.15 km. With the exception of some curvature at the higher offsets, all the reflection events have been flattened.

The stacked image after migration is shown in Figure 5. The structural boundaries of the true model are plotted on top of it. Except at the edges of the model where there is no shot coverage, the seismic image is accurate within the seismic resolution: the boundaries all lie on the seismic wavelet after migration. This means that boundaries can be picked from the migrated image, even though the used velocity function is a smooth representation of the true velocity model. The picked boundaries are used as constraints in the determination of structural velocities.

Fuzzy boundaries

In the above test I have shown that boundaries can be picked after migration with a smooth velocity model. The errors made are small and fall within the seismic resolution. Nevertheless, to avoid errors in the second velocity optimization, we may define "fuzzy" boundaries (Figure 6). Instead of a sharp jump in velocity at a boundary, we define a boundary as a region with the width of the seismic resolution (about half the seismic wavelength) in which a smooth velocity "curvature" exists.

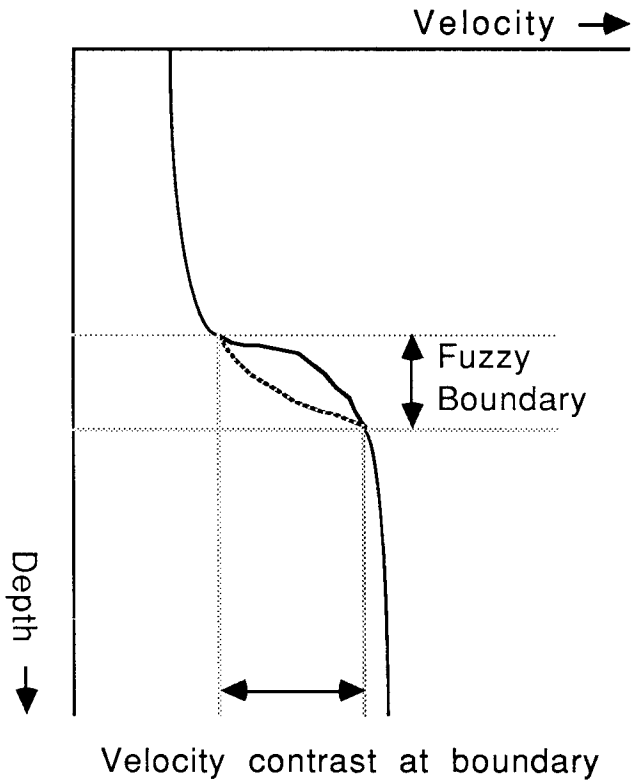

FIG. 6. A fuzzy boundary is a region with the width of the seismic resolution, in which the velocity is smoothly varied. The dashed line shows an alternative velocity variation in the boundary.

The velocities in the boundaries are included as parameters in the structural-model optimization. Picking errors will not bias the determination of structural velocities in this way: the inverted velocity model must be consistent with all traveltime information; local picking errors can only be explained by local velocity variations in the boundaries.

The variation in resolution of the boundaries in the seismic image is taken into account during the interpretation: if there are ill-defined boundaries in the image, the width of the boundaries is increased. In an automatic picking scheme this can be done by not just picking one peak or through in the wavelet, but also neighboring peaks or throughs.

Note that the introduction of fuzzy boundaries does not mean that the velocity model is made smooth again: I do allow sharp velocity contrasts between structures, the smooth change of velocity in the boundaries is just a way to prevent picking errors from affecting the velocities in the structures.

DETERMINATION OF STRUCTURAL VELOCITIES

The geological interpretation described above provides information that constrains the determination of structural velocities. First, the picked boundaries are used to parametrize the velocity model in separate structures, each of which has a velocity function that is independent of the others. The fuzzy boundaries are treated as an extra structure. Second, well logs and geological knowledge of specific structures further constrain the velocity model. These observations are quantified by a damping matrix that limits the change in the velocity parameters during the optimization.

Structural tomography

Cumulative traveltime is the time needed for a ray to travel from a shot to a given reflector and from the reflector back to a geophone. In the first optimization (the migration-velocity analysis with a smooth model), we try to find the right position of the reflectors. By adjusting a smooth velocity model, we attempt to match the cumulative traveltimes to reflectors calculated with the model with the ones found in the data. Consequently, cumulative traveltimes are available at almost no extra cost after the first optimization: if we have used Kirchhoff migrations in the migration-velocity analysis, we have saved the traveltimes; otherwise the traveltimes can be easily calculated by ray tracing through the smooth velocity model.

From the interpretation of the seismic image boundaries are determined where the velocity is discontinuous. The velocities inside the structures can now be found by a tomographic method. To allow the velocities to vary continuously inside the structures (as is often found inside seismic sequences), the velocities are modeled by splines. The coefficients of the splines are the parameters that need to be estimated by an iterative tomographic method. The combination of migration and tomography is also used by Stork and Clayton (1987), but there some differences between their approach and mine. First, I have fixed the depth of the reflectors by geological interpretation, thereby avoiding the problem of depth-velocity ambiguity. Second, I use splines instead of a gridded model, leading to a drastic reduction in the number of mapped parameters. I thus prevent the system of equations from becoming underdetermined. This latter problem forces Stork and Clayton to damp their inversion heavily by imposing smoothness constraints on the velocity field. While I explicitly smooth the velocity field by using splines, the smoothness is constrained to those regions where geology tells me that there are no large velocity contrasts.

Parametrization of structural-velocity model

The geological interpretation of the seismic image defines a number of structures. The position of the structures in the model are described by step functions

$$H_i(x,z) = \begin{cases} 1 & \text{if } (x,z) \text{ lies in structure } i \ (i = 1, NS+1), \\ 0 & \text{elsewhere.} \end{cases} \tag{1}$$

NS is the number of structures identified in the interpretation; the $(NS + 1)$th structure contains the fuzzy boundaries. The step functions are called templates for reasons that will become clear later.

The velocities in the structures vary smoothly, and are independent of each other. However, rather than using velocity as variable in the inversion, slowness is used because the relation between slowness and traveltimes can better be linearized than the one between velocity and traveltimes. The slowness field in each structure is modeled by cubic B-splines. The total slowness function, $w(x, z)$, is then defined as follows:

$$w(x,z) = \sum_{i=1}^{NS+1} \sum_{j=1}^{NX} \sum_{k=1}^{NZ} c_{ijk}\, H_i(x,z)\, F_j(x)\, G_k(z), \tag{2}$$

with NX and NZ the number of spline knots in the x- and z-direction. F_j and G_k are the spline functions at the jth knot in the x-direction and the kth knot in the z-direction, respectively (see Inoue, 1986).

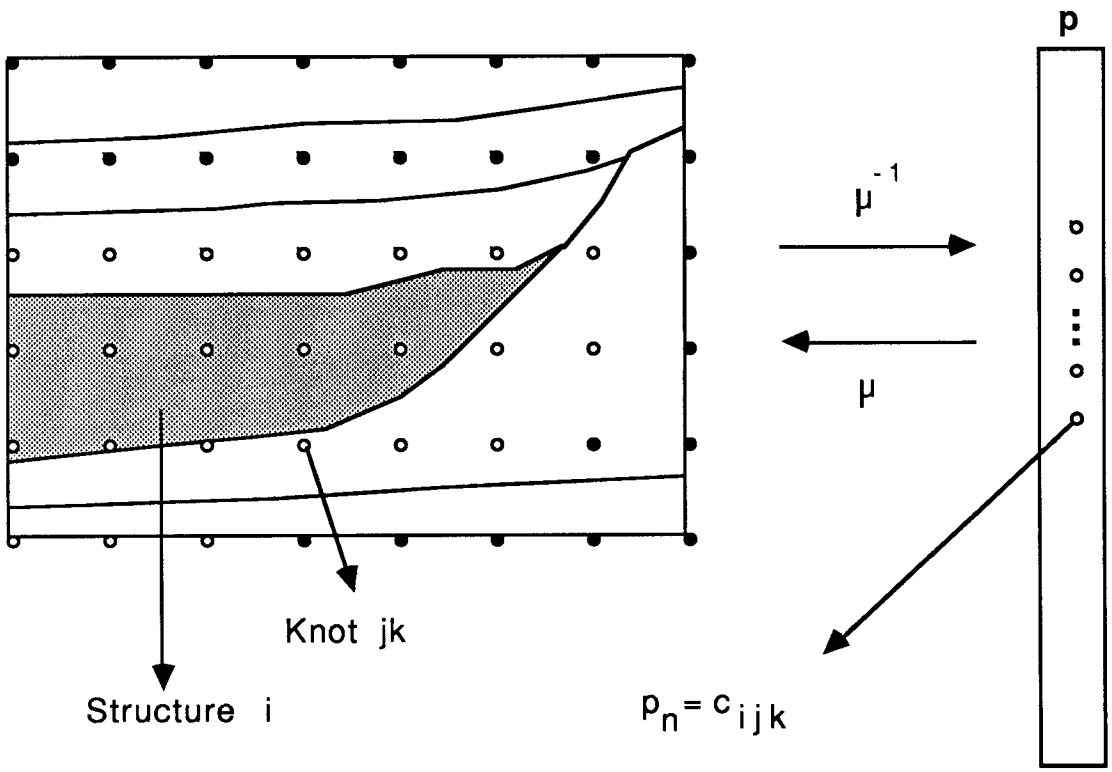

FIG. 7. Mapping of spline coefficients of different structures in one parameter vector. The structure map on the left-hand side is the result of structural interpretation. The dots denote knots of the spline functions. The spline coefficients at the knots in each structure are mapped into the parameter vector $\mathbf{p}$, using the inverse of the mapping function μ^{-1}. The open dots show knot positions of spline functions that model the velocity in the highlighted structure. Note that some knots outside the structure also control the velocity.

The parameters in the inversion are the spline coefficients, c_{ijk}. Formally, the number of parameters is $(NS + 1) \cdot NX \cdot NZ$, but in practice not all of them

are needed in the inversion: only the coefficients at spline knots that lie inside a given structure contribute to the slowness field for that structure. Therefore, the templates $H_i(x,z)$ are used to map the coefficients c_{ijk} into one parameter vector $\mathbf{p}$ (see also Figure 7). A coefficient c_{ijk} is only added to the vector if ijk is such that the jkth spline knot lies in structure i. Hence, the elements p_n of the vector $\mathbf{p}$ satisfy

$$p_n \;=\; c_{\mu(n)}, \quad n = 1, N, \tag{3}$$

where the mapping function μ transforms the index n of the parameter vector to 3 indices ijk; its inverse, μ^{-1}, does the opposite:

$$\begin{cases} \mu(n) & = ijk \\ \mu^{-1}(ijk) & = n \end{cases} \;; \quad \forall\, ijk:\; H_i(x,z) \;=\; 1 \;\wedge\; F_j(x)\; G_k(z) \;\neq\; 0. \tag{4}$$

The number of mapped parameters, N, is larger than $NX \cdot NZ$, because the spline knots for different structures overlap at the boundaries. However, N generally does not exceed $2 \cdot NX \cdot NZ$.

Forward modeling and linearization

The traveltime of a ray can be described as an integral over the slowness along its path

$$t_m \;=\; \int_0^{S_m} w(x(s), z(s))\; ds. \tag{5}$$

Here s is the arclength, m is the ray-index, and S_m the total arclength for ray m. Substitution of the expression for $w(x,z)$ (equation (2)) gives

$$\begin{aligned} t_m \;&=\; \int_0^{S_m} \sum_{i=1}^{NS+1} \sum_{j=1}^{NX} \sum_{k=1}^{NZ} c_{ijk}\; H_i(x(s),z(s))\; F_j(x(s))\; G_k(z(s))\; ds \\ &=\; \sum_{i=1}^{NS+1} \sum_{j=1}^{NX} \sum_{k=1}^{NZ} c_{ijk} \int_0^{S_m} H_i(x(s),z(s))\; F_j(x(s))\; G_k(z(s))\; ds \\ &=\; \sum_{i=1}^{NS+1} \sum_{j=1}^{NX} \sum_{k=1}^{NZ} c_{ijk} \int_0^{S_m} L_{ijk,m}(s)\; ds \\ &=\; \sum_{n=1}^{N} p_n\; A_{n,m}\;, \end{aligned} \tag{6}$$

where $A_{n,m}$ is the mth row of the forward modeling matrix; the parameter index n is found by the mapping function (equation (4)):

$$A_{n,m} \;=\; \int_0^{S_m} L_{\mu(n),m}(s)\; ds \;=\; \int_0^{S_m} L_{ijk,m}(s)\; ds, \tag{7}$$

with:

$$L_{ijk,m}(s) = H_i(x(s),z(s))\; F_j(x(s))\; G_k(z(s)). \tag{8}$$

For M rays a M-dimensional vector $\mathbf{t}$ of traveltimes is found, and equation (6) becomes

$$\mathbf{t} = \mathbf{A}\,\mathbf{p}. \tag{9}$$

The ray paths are calculated with a ray-tracing method that solves the system of ray equations by a 4th-order Runge-Kutta integration (see Van Trier, 1988a). The matrix $\mathbf{A}$ is calculated similarly: the elements $L_{ijk,m}(s)$ are included as ray variables in the ray equations, and their numerical integration yields $\mathbf{A}$.

Inversion

The goal of the inversion is to find a structural velocity model for which traveltimes of rays going from the surface to the reflectors are the same as for the smooth model. Instead of tracing rays down from the surface, rays are traced up from the reflectors, though, because of two numerical reasons. First, checking if a ray arrives at the surface (a straight line) is easier than checking if a ray arrives at a reflector (a curve). Second, interpolating traveltimes of rays with endpoints on a straight line is easier than of rays with endpoints on a curve.

For all reflectors (identified in the geological interpretation), ray fans are traced from MS selected points on the reflector to points at the surface. The surface points correspond to geophone locations, with the number of points (MR) limited by the minimum and maximum offset in the data. The ray-tracing method is not two-point (Van Trier, 1988a), and, consequently, rays will not arrive exactly at the surface points. However, selecting the ray nearest to the surface point is accurate enough for the construction of the matrix $\mathbf{A}$. Traveltimes are found by quadraticly interpolating traveltimes of the 3 rays with endpoints nearest to the surface point. Crossing rays are normally not included in the inversion. Summarizing, for a reference structural model $\mathbf{p_0}$, a matrix $\mathbf{A_0}$ is constructed and a traveltime vector $\mathbf{t_0}$ is calculated as described above:

$$\mathbf{t_0} = \mathbf{A_0}\,\mathbf{p_0}. \tag{10}$$

$\mathbf{t_0}$ is a M-dimensional vector with $M = MR \cdot MS$.

Traveltimes for the smooth model are also calculated by ray tracing, or they are selected (or interpolated) from traveltimes used in the smooth-model optimization. These traveltimes form the datavector $\mathbf{t_s}$. The optimization objective is to perturb the reference model such that traveltimes through the perturbed model $\mathbf{p_s}$ (where $\mathbf{p_s} = \mathbf{p_0} + \delta\mathbf{p}$) match the traveltimes through the smooth model:

$$\mathbf{t_s} = \mathbf{A_s}\,\mathbf{p_s}. \tag{11}$$

$\mathbf{A_s}$ is the matrix calculated for $\mathbf{p_s}$. The problem is that $\mathbf{p_s}$ is unknown, and thus it is impossible to calculate $\mathbf{A_s}$. However, assuming the perturbations $\delta\mathbf{p}$ to be small, Fermat's principle can be applied and the reference matrix $\mathbf{A_0}$ can be used to calculate traveltimes:

$$\mathbf{t_s} \simeq \mathbf{A_0}\,(\mathbf{p_0} + \delta\mathbf{p}) = \mathbf{A_0 p_0} + \mathbf{A_0}\delta\mathbf{p} = \mathbf{t_0} + \mathbf{A_0}\delta\mathbf{p} \tag{12}$$

Using $\delta \mathbf{t} = \mathbf{t_s} - \mathbf{t_0}$, this equation becomes

$$\delta \mathbf{t} = \mathbf{A_0}\, \delta \mathbf{p}. \tag{13}$$

Equation (13) is solved by least squares:

$$\delta \mathbf{p} = (\mathbf{A_0^T A_0})^{-1}\, \mathbf{A_0^T}\, \delta \mathbf{t}. \tag{14}$$

I use the conjugate gradient solver LSQR (Paige and Saunders, 1982) to solve the least-squares problem. Several non-linear iterations are normally needed before the inversion converges: at each iteration the model is updated and the matrix is recalculated by ray tracing through the updated model.

Damping by geological constraints

In tomography, $\mathbf{A_0^T A_0}$ is often singular and the least-squares problem usually must be damped to get a meaningful solution. This can be done by adding $\mathbf{D}\delta\mathbf{p} = 0$ as data to the system of equations (13):

$$\begin{pmatrix} \mathbf{A_0} \\ \mathbf{D} \end{pmatrix} \delta \mathbf{p} = \begin{pmatrix} \delta \mathbf{t} \\ 0 \end{pmatrix} \tag{15}$$

and solving the least-squares problem for this new system. The damping matrix $\mathbf{D}$ can have different forms, the simplest being a diagonal matrix, where the diagonal elements are inversely proportional to the parameter variance. The elements are normally set to values corresponding to a priori expectations of the amount of variation in the parameters.

Here the determination of $\mathbf{D}$ is guided by geological knowledge: when velocities can be determined from well logs, the variance is set to zero for parameters that control the velocity at the borehole, and is slowly increased for parameters controlling the velocity away from the hole.

If dip information is available, a more complicated damping matrix can be constructed that favors certain dip directions. For a structure with dip ϕ, a dip vector can be defined as $\mathbf{\Delta} = (d_x\ d_z)^T = (\cos\phi\ \sin\phi)^T$. If the velocity gradients in the structure follow the dip, the slowness function w will satisfy

$$-d_z \frac{\partial w}{\partial x} + d_x \frac{\partial w}{\partial z} = -\sin\phi \frac{\partial w}{\partial x} + \cos\phi \frac{\partial w}{\partial z} = 0 \tag{16}$$

This constraint is incorporated in the inversion by setting the damping matrix to a linear combination of the matrix $\mathbf{D}_x$, representing the velocity derivative with respect to x, and the matrix $\mathbf{D}_z$, representing the z-derivative. The nth row of the derivative matrix determines the velocity derivative at the nth spline knot. The derivative matrices are calculated by taking the derivatives of the spline functions. At all spline knots dip vectors are estimated, forming two diagonal matrices: $\mathbf{\Delta}_x$

for the lateral components, $\mathbf{\Delta}_z$ for the depth components. Equation (16) can then be written as:

$$\mathbf{D} = -\mathbf{\Delta}_z\mathbf{D}_x + \mathbf{\Delta}_x\mathbf{D}_z. \tag{17}$$

By adding the damping equations $\mathbf{D}\delta\mathbf{p} = 0$ to equation (13), velocity gradients along the dip directions (which satisfy the damping equations) are preferred above other gradients.

Results

The structural tomography is applied to the intrusion model of Figure 2a. As was shown before, the seismic image after migration with the smooth model of Figure 2b is accurate enough to pick boundaries. These boundaries are now used to parametrize the structural velocity model. The velocities in each structure are modeled by spline functions with 26 spline knots in the depth as well as the lateral direction. As an extra geological constraint, the velocity of the salt structure is assumed to be known. The idea behind this assumption is that a salt structure is generally recognizable in the seismic image, and that salt velocities are often known from observations at other salt structures in the same sedimentary basin.

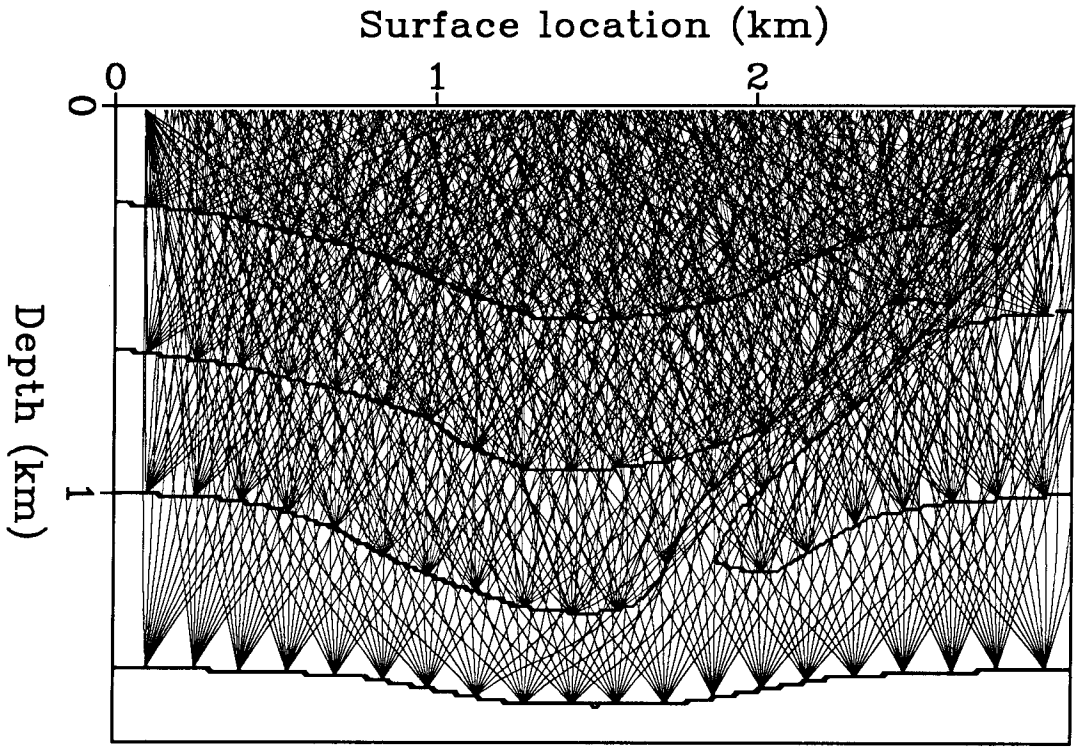

FIG. 8. Ray coverage in structural tomography. Rays are traced up from 80 points on the reflector to 100 points on the surface. The lateral coordinates of the surface points are centered around the lateral position of the reflector point. For display purposes, the ray fans are subsampled by a factor of 10.

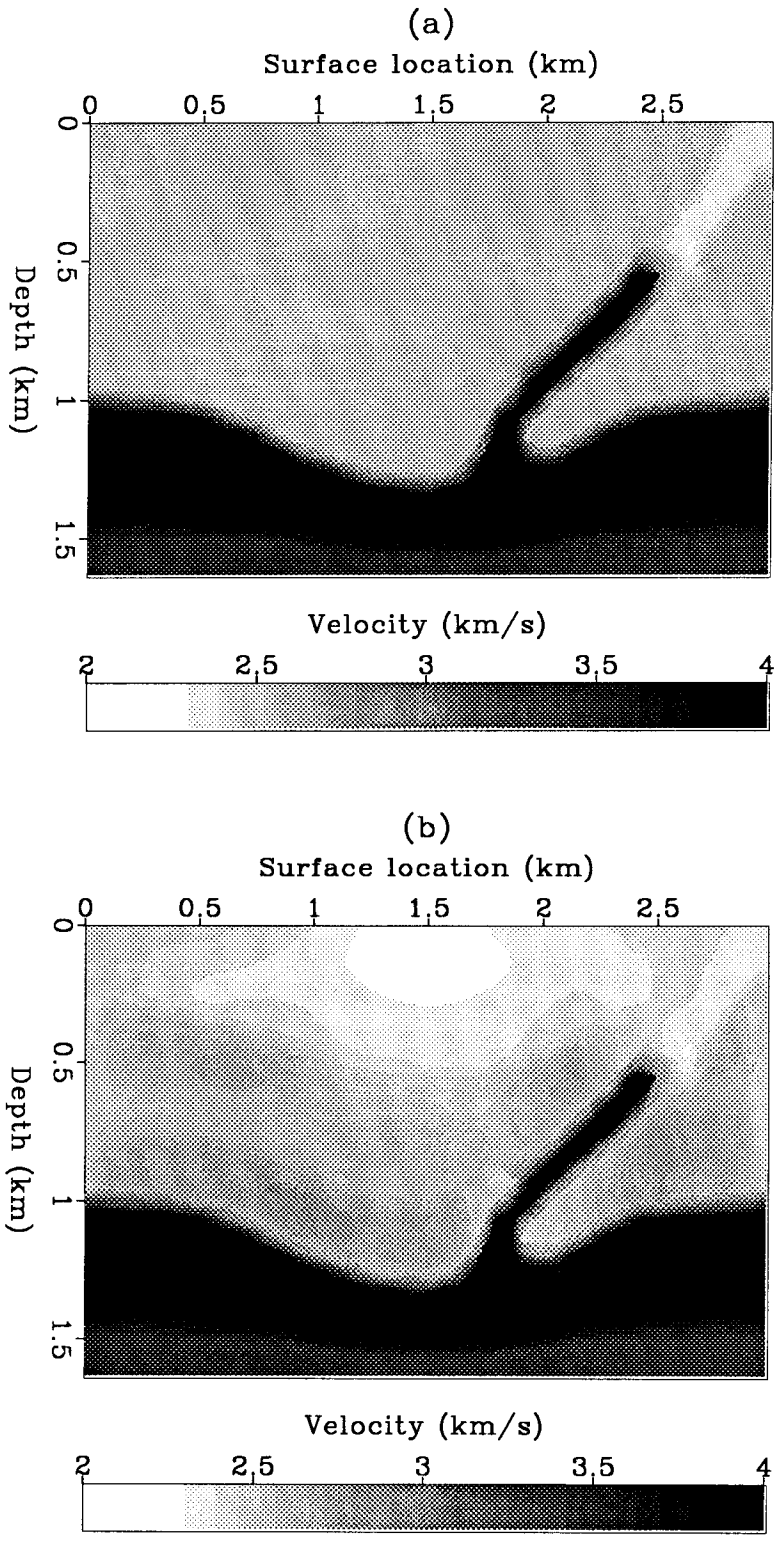

FIG. 9. Result of structural tomography: (a) starting model; (b) after one non-linear iteration.

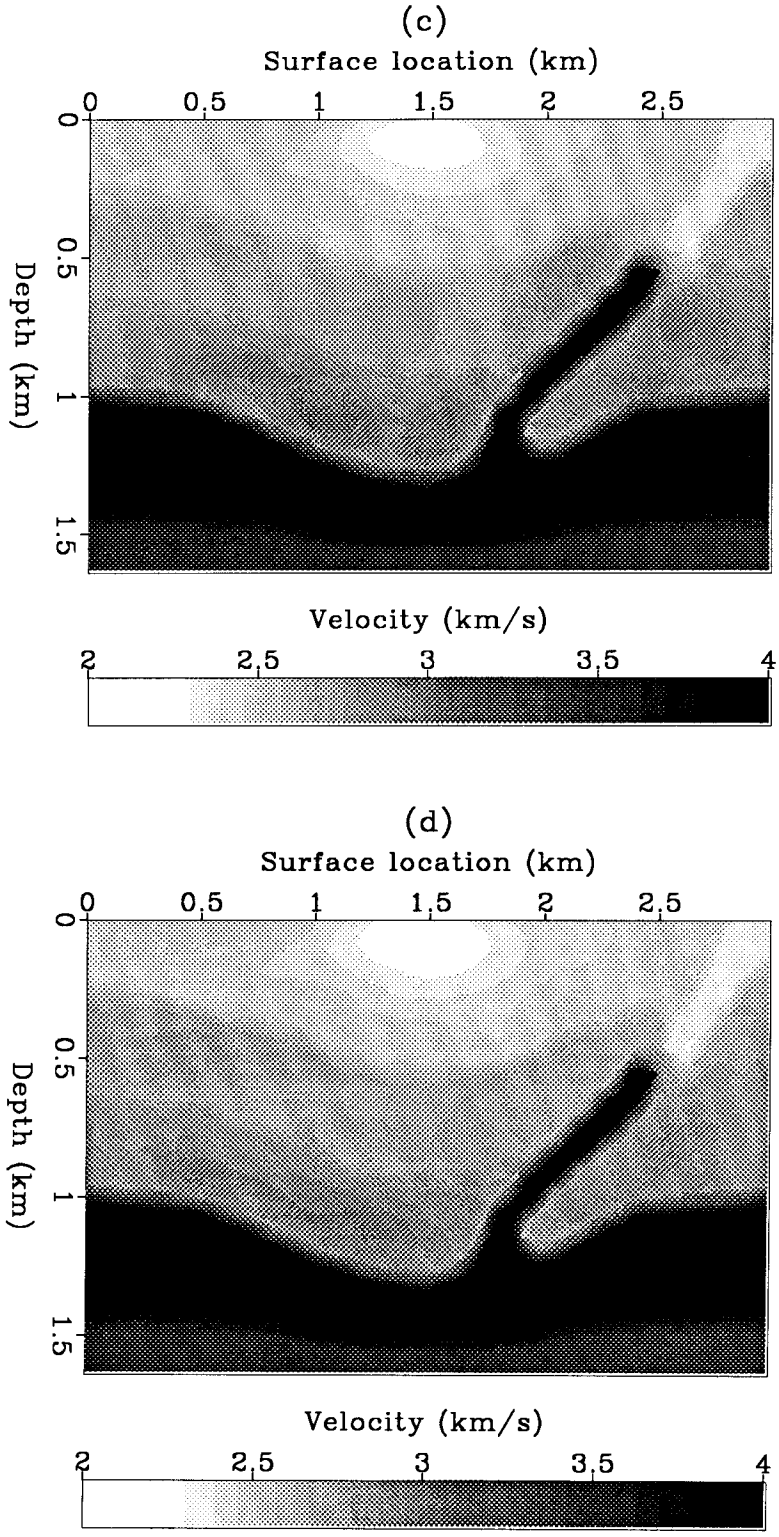

FIG. 9. Result of structural tomography: (c) after two non-linear iterations; (d) after three iterations.

Rays are traced through the smooth model to determine traveltimes from reflectors to the surface. Figure 8 shows the ray fans used in the inversion. The total number of rays is 8000: 80 ray fans with rays arriving at 100 surface points. At the start of the inversion, the velocities in all the structures are set to 2.6 km/s, except for the salt structure which has the correct velocity (Figure 9a). Figures 9b, c, and d show the result after one, two and three non-linear iterations in the inversion, respectively (see also color plot (Figure 10) at the end). At each iteration the forward-modeling matrix is recalculated by ray tracing through the updated model. In this example the damping matrix is a diagonal matrix; I have not yet tested the inversion with other damping matrices. After three iterations, increasing the number of iterations does not change the result much.

The inverted result matches well the true model: the low-velocity region in the top structure is recovered, although it is somewhat broader than in the true model. The inverted velocities in the structures also correspond to the true velocities.

Although the smooth model explains the cumulative traveltimes as well as the structural model, the structural model is more useful than the smooth model. Velocity contrasts are put at places where geology dictates it, and, likewise, velocities are kept smooth at locations where no large jumps in velocities are expected. In this fashion, the structural model provides more information about the actual velocities than the smooth model does.

CONCLUSIONS

I have presented a method that includes geological information in the seismic velocity estimation. The first part of the method is concerned with determining a well-focused image. The image is obtained by migration with a smooth-velocity model. Then, structural tomography combines the high-wavenumber information in the migrated image with the low-wavenumber information in the smooth-velocity model into one structural-velocity model. Where seismic data do not provide information (e.g., at regions between reflectors), the velocity model is determined by geological constraints, coming from well logs, or general geological knowledge.

Several aspects of the method remain to be investigated. First, the effect of mispicked boundaries on the velocity inversion has to be tested, where the question is whether fuzzy boundaries can indeed prevent picking errors from biasing structural velocities. Second, a "geological" damping matrix that uses well log and dip information has to be included in the inversion.

Work is under way to implement the geological interpretation on an interactive workstation. The boundaries, together with their width, are then interactively picked on the workstation. After the structural-velocity estimation, a detailed interactive analysis of selected parts of the migrated data can be used to refine the structural model (Van Trier, 1988b).

ACKNOWLEDGMENTS

I would like to thank Biondo Biondi, John Etgen and Marta Woodward for many interesting discussions. I thank Shell International Petroleum Maatschappij B.V. for financial contributions.

REFERENCES

Al-Yahya, K., 1987, Velocity analysis by profile migration: Ph.D. thesis, Stanford University.

Biondi, B., 1988, Interval velocity estimation from beam stacked data—an improved method: SEP–**57**.

Etgen, J., 1987, Velocity analysis by iterative depth migration: a proposal: SEP–**51**, 157–174.

Fowler, P., 1985, Migration velocity analysis by optimization: linear theory: SEP–**44**, 1–20.

Fowler, P., 1986, Extending Toldi's velocity analysis algorithm to include geologic structure: SEP–**44**, 1–20.

Inoue, H., 1986, A least-squares smooth fitting for irregularly spaced data: finite-element approach using the cubic B-spline basis: Geophysics, **51**, 2051–2066.

Paige, C., and Saunders, M., 1982, LSQR: an algorithm for sparse linear equations and sparse least squares: ACM Trans. Math. Softw., **8**, 43–71.

Stork, C., and Clayton, R., 1987, Application of tomography to two data sets containing lateral velocity variation: Presented at the 57th Ann. Internat. Mtg., Soc. Explor. Geophys.

Sword, C., 1987, CDR tomographic velocity analysis: Ph.D. thesis, Stanford University.

Van Trier, J., 1987, Velocity analysis by nonlinear optimization of phase-contoured shot profiles: SEP–**51**, 85–106.

Van Trier, J., 1988a, Vectorized initial-value ray tracing for arbitrary velocity models: SEP–**57**.

Van Trier, J., 1988b, High-resolution velocity inversion of o migrated data after structural interpretation: SEP–**57**.

Van Trier, J., 1988c, Non-linear velocity estimation: field data addendum: SEP–**57**.

FIG. 10. Color plot of results: structural model (*upper left*); smooth model (*upper right*); starting model (*middle left*); result after one iteration (*middle right*); after two iterations (*bottom left*); after three iterations (*bottom right*).

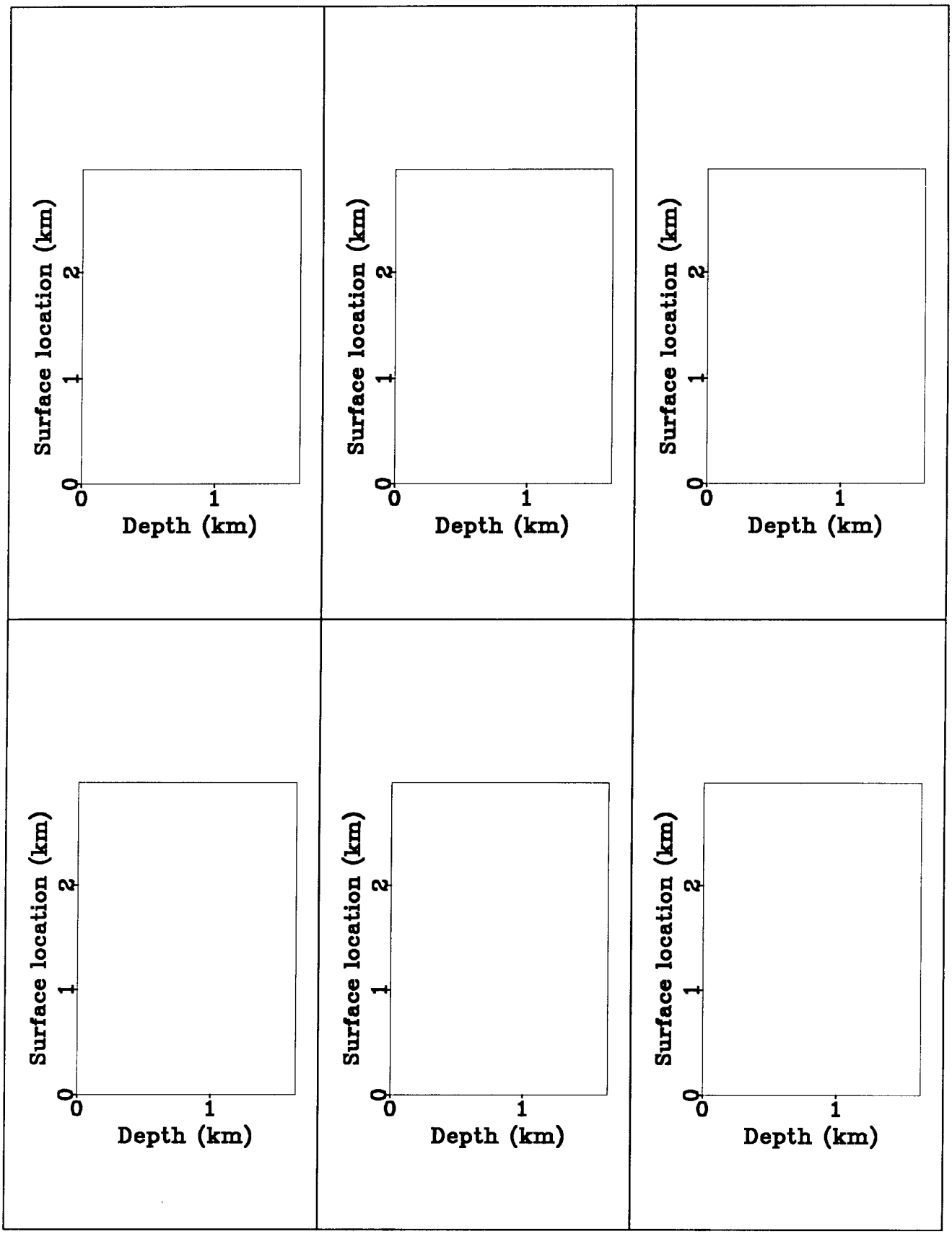
Surface location (km)
0
1
2
0
1
Depth (km)